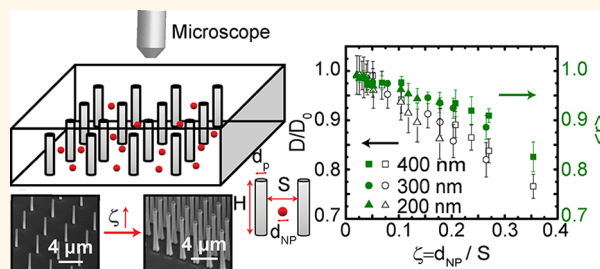


Diffusive Dynamics of Nanoparticles in Arrays of Nanoposts

Kai He,[†] Firoozeh Babaye Khorasani,[†] Scott T. Retterer,[‡] Darrell K. Thomas,[§] Jacinta C. Conrad,^{†,*} and Ramanan Krishnamoorti^{†,*}

[†]Department of Chemical and Biomolecular Engineering, University of Houston, Houston, Texas 77204-4004, United States, and [‡]Center for Nanophase Materials Sciences and BioSciences Divisions and [§]Center for Nanophase Materials Sciences, Oak Ridge National Laboratory, Oak Ridge, Tennessee 37934, United States

ABSTRACT The diffusive dynamics of dilute dispersions of nanoparticles of diameter 200–400 nm were studied in microfabricated arrays of nanoposts using differential dynamic microscopy and single particle tracking. Posts of diameter 500 nm and height 10 μm were spaced by 1.2–10 μm on a square lattice. As the spacing between posts was decreased, the dynamics of the nanoparticles slowed. Moreover, the dynamics at all length scales were best represented by a stretched exponential rather than a simple exponential. Both the relative diffusivity and the stretching exponent decreased linearly with increased confinement and, equivalently, with decreased void volume. The slowing of the overall diffusive dynamics and the broadening distribution of nanoparticle displacements with increased confinement are consistent with the onset of dynamic heterogeneity and the approach to vitrification.



KEYWORDS: diffusion · porous media · non-Gaussian dynamics · nanoparticles

The transport properties of nanoparticles in complex confined media play a significant role in biomedical, environmental applications, and in oil and gas exploration and production. For example, therapeutic drugs encapsulated as nanoparticles must be delivered¹ and transported through the extracellular matrix² to reach targeted cells.^{3,4} Similarly, the fate of engineered nanoparticles and nanoscale contaminants in aquatic systems depends in part on their transport properties in environmental porous media such as saturated soils⁵ or biofilms.^{6,7} Finally, nanoparticles developed for use in enhanced oil recovery applications^{8,9} must be designed for transport through highly confined pore throats, especially in low permeability reservoirs.

Confining a micrometer-sized colloidal particle changes its transport properties: particles near walls¹⁰ or in enclosed chambers¹¹ diffuse more slowly than those in bulk. As the size of the particles is decreased below one micrometer, however, the effects of electrostatic¹² and hydrodynamic^{13,14} interactions on dynamics become more pronounced. Moreover, natural porous media are extremely heterogeneous: pore

diameters range from nanometers to millimeters, pores can be connected or disconnected, and the surface properties of the pores can vary in chemistry and in wettability. As a result, heterogeneities in confinement, pore connectivity, and porous media–nanoparticle interactions can introduce different physical mechanisms for transport that generate a wide variety of transport properties observed for nanomaterials in complex media.^{15–23}

One route toward an improved fundamental understanding of transport mechanisms is to create simplified models of porous media.²⁴ Specifically, recent advances in self-assembly and microfabrication have generated model media in which the pore structure and wettability are precisely controlled, for example including inverse opals^{25,26} and microfabricated²⁷ and nanofabricated²⁸ post arrays. These model media exhibit uniform and mono-dispersed pore sizes and spacings. By eliminating variations in pore connectivity and surface chemistry, these simplified model media reduce heterogeneity and thereby enable microscopic studies that isolate the effects of well-defined confinement on the transport properties of nanoparticles.

* Address correspondence to ramanan@uh.edu; jcconrad@uh.edu.

Received for review February 12, 2013 and accepted May 14, 2013.

Published online May 14, 2013
10.1021/nn4007303

© 2013 American Chemical Society

Here, we focused on transport at zero shear rate and investigated the dynamics of nanoparticles diffusing in nanopost arrays. We fabricated arrays of nanoposts with a diameter of 500 nm arranged on a square lattice with spacing of 1.2–10 μm using an electron-beam lithography process. The dynamics of nanoparticles of diameter ranging from 200 to 400 nm diffusing in these media were measured using differential dynamic microscopy and single-particle tracking. As the nanoparticles were increasingly confined by the array of posts, we found that the image structure function could not be fit by a single exponential but instead was best fit by a stretched exponential function. The relative diffusivity and the stretching exponent extracted from the stretched exponential fits decreased approximately linearly as the void fraction of the nanopost array was decreased or as the ratio between the particle diameter and nanopost spacing was increased. We confirmed this behavior in direct-space measurements using single-particle tracking. The slowing of dynamics is consistent with confinement of the nanoparticle by the cylindrical posts. The emergence of a spectrum of relaxation times suggests either a heterogeneous environment on a length scale comparable to the particle size or an analogy to vitrification²⁹ of the nanoparticles in confined geometries.

RESULTS AND DISCUSSION

We collected time-resolved fluorescence optical micrographs for the 200 to 400 nm nanoparticles diffusing in the bulk and in microfabricated post arrays (Figure 1) with post spacing ranging from 1.2 to 10 μm corresponding to a void fraction (θ) range of 0.76 to 1 and a confinement parameter (ζ) range of 0 to 0.35. From time series of fluorescence images, we calculated the delay-time dependence of the azimuthally averaged image structure function $D(q,\Delta t)$.

For each wavevector q , the magnitude of $D(q,\Delta t)$ increased with increasing delay time Δt , as shown in Figure 2, indicating that the positions of nanoparticles became increasingly uncorrelated from their original positions with increasing Δt . For particles diffusing in the bulk and in large spacing post arrays (Figure 2a–c), $D(q,\Delta t)$ reached a plateau at long Δt , whereas for those diffusing in the small spacing post arrays (Figure 2d,e), no plateau was observed even at the longest delay times accessed in these experiments. Nonetheless, the temporal evolution of the structure function for these confined cases exhibited at least two distinctive dynamic events. We attributed the fastest of these events to the diffusive dynamics of the nanoparticles in the confined media. We were unable to reasonably capture the longer dynamics in the structure function data in these experiments. Because the slower dynamical event was not observed in confined media at small values of the wavevector q (Figure 2f), we attributed the changes in $D(q,\Delta t)$ on long time scales, observed at

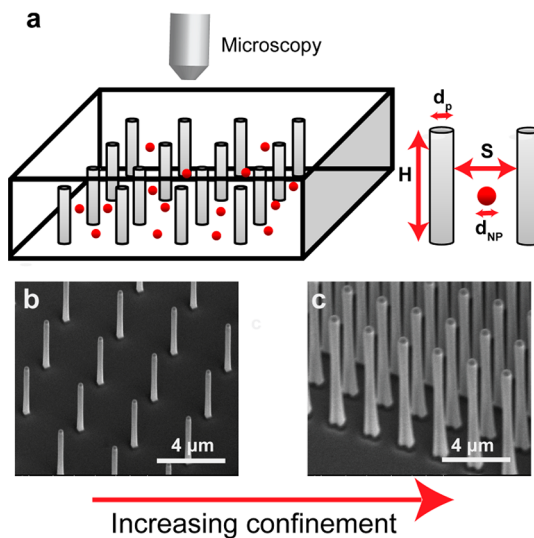


Figure 1. (a) Schematic of cylindrical post arrays filled with polystyrene nanoparticle dispersions. (b, c) Scanning electron micrographs of posts of diameter $d_p = 500 \text{ nm}$, (b) height $H = 10 \mu\text{m}$ and spacing $S = 6 \mu\text{m}$, and (c) height $H = 11.9 \mu\text{m}$ and spacing $S = 1.6 \mu\text{m}$.

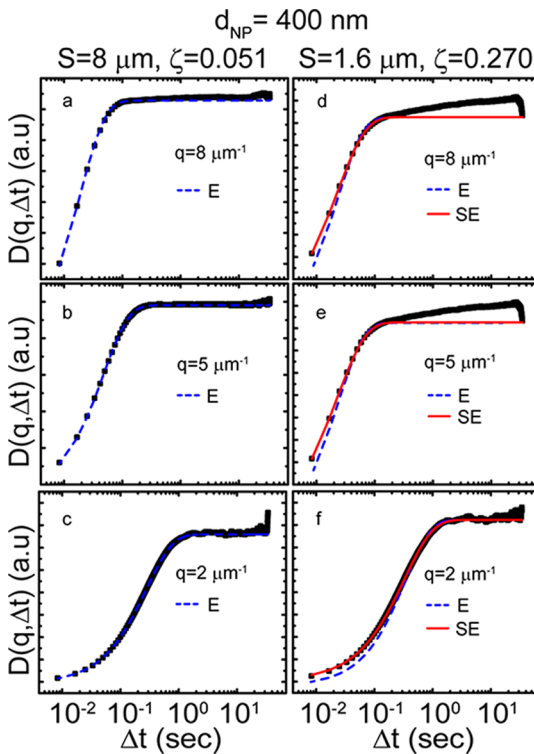


Figure 2. Structure function $D(q,\Delta t)$ as a function of delay time Δt at $q = 8 \mu\text{m}^{-1}$ (a, d), $q = 5 \mu\text{m}^{-1}$ (b, e), and $q = 2 \mu\text{m}^{-1}$ (c, f) for 400 nm diameter nanoparticles diffusing in two different post arrays using fluorescence DDM. Panels (a), (b), and (c) present data obtained for a post spacing $S = 8 \mu\text{m}$, $\zeta = 0.051$; panels (d), (e), and (f) present data obtained for $S = 1.6 \mu\text{m}$, $\zeta = 0.270$. Dashed blue lines (notated as E) represent fits to a simple exponential model eq 1, and solid red lines (notated as SE) represent fits to a stretched exponential model (eq 2).

large q for confined samples, to the dynamics corresponding to the jump between two “caged” domains or

to the weak, possibly apolar or weakly polar, interactions between the particles and the post arrays.

We previously showed³⁰ that the image structure functions $D(q, \Delta t)$ obtained using brightfield and fluorescence DDM for 200–400 nm diameter nanoparticles in unconfined Newtonian media were excellently fitted using a single exponential model:

$$D(q, \Delta t) = A(q) \left[1 - \exp - \left(\frac{\Delta t}{\tau(q)} \right) \right] + B(q) \quad (1)$$

where $\tau(q)$ is a q -dependent relaxation time and $A(q)$ and $B(q)$ are fitting parameters that depend on the wavevector q and on the optical train. This functional form also produced good fits of the short time scale image structure function $D(q, \Delta t)$ for particles that were only weakly confined by posts ($S = 8 \mu\text{m}$), as shown by the dashed lines in Figure 2a–c. By contrast, the delay time dependence of $D(q, \Delta t)$ for particles diffusing in highly confined post arrays ($S = 1.6 \mu\text{m}$) could not be captured by the single exponential model, as shown by the dashed lines (single-exponential fit) in Figure 2d–f. These data required a new fitting model. We note that the Kohlrausch–Williams–Watts function, which incorporates a stretched exponential term (*i.e.*, $\exp[-((\Delta t)/(\tau(q))^{r(q)})]$) instead of the single exponential term applied in eq 1, has been successfully used to describe the slowing of dynamics in complex glassy³¹ and polymeric³² systems. To characterize the fast dynamic process, we thus fitted all structure functions for particles diffusing in confined nanopost arrays over a limited range of delay times to a single stretched exponential model,

$$D(q, \Delta t) = A(q) \left[1 - \exp - \left(\frac{\Delta t}{\tau(q)} \right)^{r(q)} \right] + B(q) \quad (2)$$

and extracted four parameters: the signal prefactor $A(q)$, the background $B(q)$, the q -dependent relaxation time $\tau(q)$, and the stretching exponent $r(q)$. We chose to fit the data over a delay time range that extended up to five times the relaxation time as a typical cutoff value; using higher cutoff values did not substantially alter the results that we report here. Using this protocol, the short time dynamics for all samples could be well fitted by the stretched exponential model. From the fits to the model in eq 2, we focused on the two fitting parameters $\tau(q)$ and $r(q)$ that are most closely associated with the dynamics. As noted in a previous publication,³⁰ the signal background term $B(q)$ was only dependent on the details of the optical train.

To characterize the dynamics of nanoparticles in post arrays, we first examined the wave-vector dependence of the relaxation time $\tau(q)$, obtained by fitting the image structure function to eq 2. Over a narrow range of q values (*i.e.*, $6 \mu\text{m}^{-1} < q < 8 \mu\text{m}^{-1}$) corresponding to length scales shorter than the spacing between posts, $\tau(q)$ scaled as q^{-2} for all post spacings,

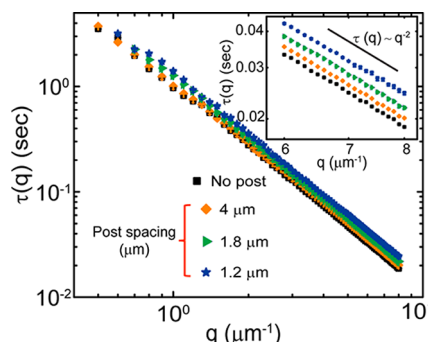


Figure 3. Relaxation time $\tau(q)$ (in seconds) as a function of the magnitude of the wave vector q (in μm^{-1}) for 400 nm nanoparticles diffusing in the bulk (black squares) and in post arrays with $S = 4 \mu\text{m}$, $\xi = 0.105$ (orange diamonds); $S = 1.8 \mu\text{m}$, $\xi = 0.237$ (olive right triangles); and $S = 1.2 \mu\text{m}$, $\xi = 0.354$ (navy stars). The inset shows that $\tau(q)$ scales as q^{-2} over the range of wavevectors from $q = 6$ to $8 \mu\text{m}^{-1}$. The error bars for $\tau(q)$ are smaller than the symbols.

as shown for representative data from 400 nm nanoparticles in Figure 3. This result indicates that the dynamics of the nanoparticles remained diffusive when moderately confined by cylindrical posts. Nevertheless, the relaxation time $\tau(q)$ at a fixed value of q increased in magnitude as the spacing between posts was decreased and the nanoparticles were increasingly confined, indicating that cylindrical obstacles (or increase in confinement) slowed the diffusive dynamics of the nanoparticles. The qualitative trends shown here for the 400 nm nanoparticles dynamics were also observed for smaller nanoparticles of diameter 200 and 300 nm (Supporting Information, Figures S2–S5).

We verified the dynamical measurements obtained using DDM by analyzing the dynamics of 400 nm nanoparticles diffusing in post arrays in real space using single particle tracking. The ensemble-averaged MSD of the nanoparticles, calculated from the trajectories, was linearly proportional to delay time Δt across the entire accessible range of delay times, as shown in Figure 4, confirming that the particle dynamics were diffusive in post arrays. We therefore extracted the average diffusion coefficient D via

$$\langle \Delta x^2(\Delta t) \rangle = 2D\Delta t \quad (3)$$

from the MSD. We note that our MSD measurements probed length scales from 0.09 to $1.2 \mu\text{m}$ and thus measured the dynamics of nanoparticles within the pores for all post spacings studied here. Furthermore, the MSD decreased as particles were increasingly confined by the posts, indicating that the particle dynamics were slowed down by the presence of obstacles or by the confinement of the nanoparticles by the posts. These observations are consistent with the results obtained from the DDM analysis in reciprocal space.

To obtain the diffusion coefficients D for the nanoparticles, we fitted the image structure function obtained via DDM to eq 2 (for nanoparticles of diameter

200, 300, and 400 nm) or the MSD obtained *via* particle tracking to eq 3 (for nanoparticles of diameter 400 nm). We compared the coefficients of nanoparticles of different diameters as a function of void fraction θ and confinement parameter ζ by normalizing all diffusion coefficients by D_0 , the diffusion coefficient for nanoparticles diffusing freely, as shown in Figure 5. We found that the diffusion coefficients extracted from the MSD were in excellent agreement with those obtained from the DDM measurement on 400 nm particles, confirming that the two analyses of the microscopy data probed the same diffusive behavior. The relative diffusivity (D/D_0) scaled linearly with θ and ζ and collapsed onto a single curve for the three different nanoparticles. The linear dependence of relative diffusivity on void fraction persisted even when the distance between posts was only of the order of three times the particle size. A similar reduction in diffusion coefficient with increase in obstacle density and linear relationship between the relative diffusivity and void fraction was observed for several cases of probe diffusion in crowded media;^{33,34} by contrast, in periodic 3-D porous media a nonlinear relationship between relative diffusivity and the confinement

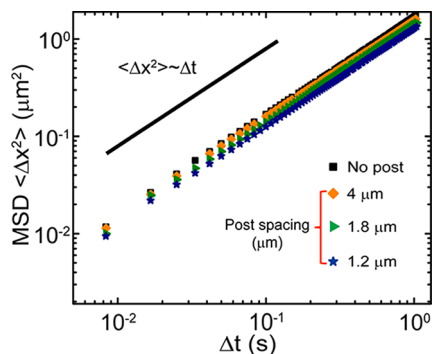


Figure 4. Mean squared displacement $\langle \Delta x^2(\Delta t) \rangle$ as a function of delay time Δt for 400 nm nanoparticles diffusing freely (black square) and in post arrays with $S = 4 \mu\text{m}$, $\zeta = 0.105$ (orange diamond); $S = 1.8 \mu\text{m}$, $\zeta = 0.237$ (olive right triangle); and $S = 1.2 \mu\text{m}$, $\zeta = 0.354$ (navy star). $\langle \Delta x^2(\Delta t) \rangle$ scales linearly as Δt across the range of delay times probed.

parameter was observed over a similar confinement range.²⁶

The diffusivities reported in Figure 5 were derived from averaged measurements of relaxation time or ensemble-averaged mean-squared displacements. The image structure function $D(q, \Delta t)$, however, was not adequately represented by a single exponential function, as would be expected for a relaxation process with a single time scale (e.g., for nanoparticles diffusing in a homogeneous medium), but was instead best modeled as a stretched exponential eq 2 with a stretching exponent $r(q)$. To gain further insight into the effect of confinement induced by the post arrays on the distribution of dynamics of the nanoparticles, we therefore examined the behavior of $r(q)$. Typically, stretched exponential behavior (*i.e.*, $r(q) < 1$) is attributed to the underlying presence of several relaxation processes with distinct relaxation times that act additively to provide the collective response observed. We found that, for a given nanoparticle diameter and a given post spacing, $r(q)$ was nearly constant over 1 order of magnitude in wavevector q (Supporting Information, Figure S6). We therefore report a single stretching exponent $\langle r \rangle$, which is a function only of the diameter of the nanoparticles and the spacing between the posts, as a function of the void fraction and confinement scale. We found that the stretching exponent $\langle r \rangle$ describing the dynamics of nanoparticles in post arrays became smaller as the spacing between the posts was decreased (that is, at smaller void fraction θ and larger confinement parameter ζ collapsed on to a single scaling curve with θ and ζ irrespective of particle size) and followed a roughly linear relationship with q and ζ (Figure 6). These results indicate that confinement modifies the distribution of the relaxation processes within the sample. A detailed description of the mathematical consequences of the relaxation described by a stretched exponential functional form³⁵ is given in the Supporting Information.

Analysis of trajectories of single particles revealed a more direct manifestation of the distribution of

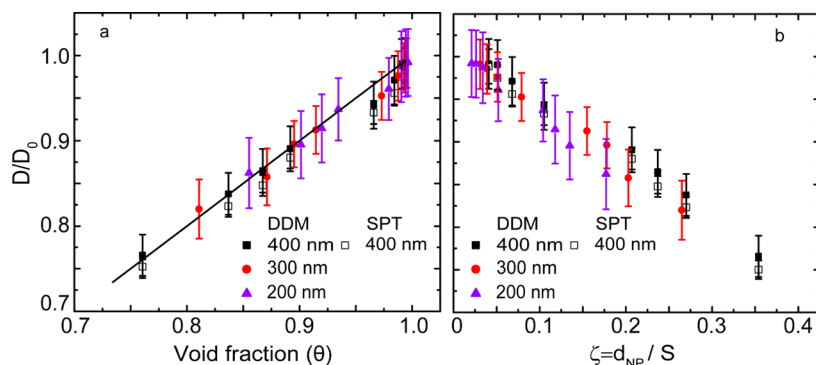


Figure 5. Relative diffusivity D/D_0 as a function of (a) void fraction θ and (b) confinement parameter $\zeta (=d_{NP}/S)$, measured by DDM (filled symbols) and single particle tracking (open symbols), for aqueous dispersions of nanoparticles of diameter of 400 (black square), 300 (red circle), and 200 nm (violet triangle). The relative diffusivity scales linearly with θ and ζ .

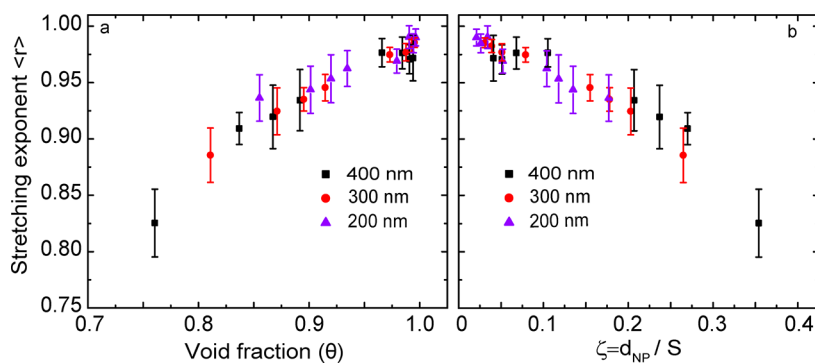


Figure 6. Stretching exponent $\langle r \rangle$ as a function of (a) void fraction θ and (b) confinement parameter $\zeta (=d_{NP}/S)$, measured by DDM for aqueous dispersions of nanoparticles of diameter of 400 (black squares), 300 (red circles), and 200 nm (violet triangles).

relaxation processes through the one-dimensional probability distribution of displacements $G_s(\Delta x, \Delta t)$, shown for representative distributions at three different delay times ($\Delta t = 0.183, 0.517$, and 0.85 s) and three different confinements in Figure 7 and in Figure S7 in the Supporting Information. For dilute uncorrelated nanoparticles in an unconfined and Newtonian medium performing a random walk, Einstein's analysis of Brownian motion indicates that the displacements of particles should follow a Gaussian distribution.³⁶ We found, however, that the distributions of displacement for the 400 nm diameter nanoparticles diffusing in post arrays deviated from a simple Gaussian, as expected for ordinary diffusion. We additionally found that $G_s(\Delta x, \Delta t)$ did not simply scale as a stretched Gaussian decay (*i.e.*, $G_s(\Delta x, \Delta t) \sim \exp[-(|\Delta x|/\gamma(\Delta t))^\beta]$). Instead, $G_s(\Delta x, \Delta t)$ was best fit to a sum of a stretched Gaussian (for long displacements) and a simple Gaussian model (for short displacements):

$$G_s(\Delta x, \Delta t) = C_1 \exp \left[-\left(\frac{|\Delta x|}{\gamma(\Delta t)} \right)^\beta \right] + C_2 \exp \left[-\left(\frac{\Delta x}{\lambda} \right)^2 \right] \quad (4)$$

where C_1 and C_2 are prefactors and $\gamma(\Delta t)$ and λ are the decay lengths for stretched Gaussian and simple Gaussian, respectively. We found that the simple Gaussian (G) exhibited a nearly constant width (Figure S8 in Supporting Information). Moreover, to minimize the number of parameters used to fit the one-dimensional probability distribution we noted that the best fits were obtained for all values of Δt with a stretching exponent β that was $\sim 2\langle r \rangle$. We therefore fixed the Gaussian stretching exponent β at $2\langle r \rangle$ and the decay length λ of the Gaussian that described the short displacement data at $0.48 \mu\text{m}$ and thereby systematically fitted the data to a single parameter model and obtained the delay time dependent decay length $\gamma(\Delta t)$. We found that this protocol allowed us to obtain good fits to $G_s(\Delta x, \Delta t)$ across the range of delay times probed in the experiment and moreover allowed us to resolve relatively small changes in the value of $\langle r \rangle$, as shown in Figure S8 in the Supporting Information.

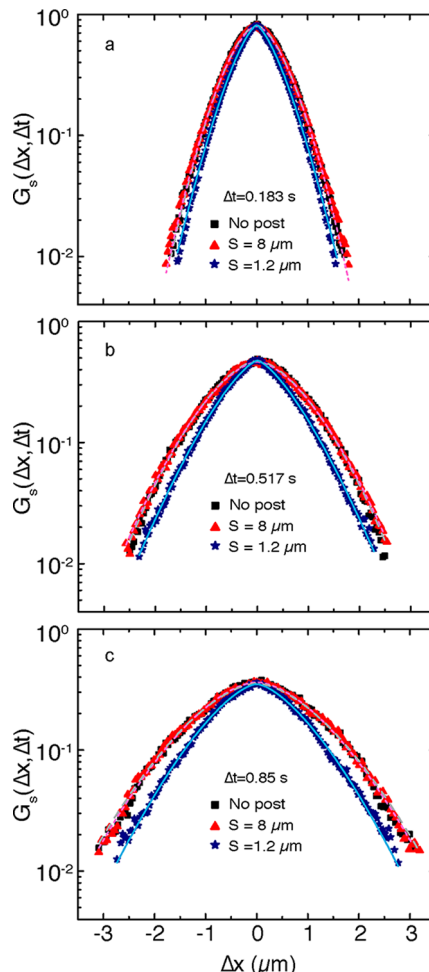


Figure 7. Probability distribution of particle displacements $G_s(\Delta x, \Delta t)$ for 400 nm particles diffusing freely and in post arrays with $S = 8 \mu\text{m}$, $\zeta = 0.051$ and $S = 1.2 \mu\text{m}$, $\zeta = 0.354$ at delay times Δt of (a) 0.183 s, (b) 0.517 s, and (c) 0.85 s, respectively. Lines indicate fits to eq 4.

The decay length $\gamma(\Delta t)$ extracted from the fits to eq 4 increased as the square root of the delay time, *i.e.*, $\gamma(\Delta t) \sim (\Delta t)^{1/2}$, as shown in Figure 8. We note that the stretched Gaussian can be interpreted as a sum of Gaussian distributions, with a distribution of relaxation times and processes,^{35,37} with the reported diffusion coefficient an averaged quantity over this distribution

(as shown explicitly in the Supporting Information). The decay length scale $\gamma(\Delta t)$ thus represents a mean characteristic length scale that is an average of the length scales associated with each of the relaxation processes that contribute to the stretched exponential distribution of displacements. The observed delay time scaling of $\gamma(\Delta t)$ suggests that each relaxation process is diffusive in origin, with the distribution of relaxation times reflecting the heterogeneity in the environment,^{38,39} perhaps due to proximity of the posts. This argument is consistent with the diffusive character of the average dynamics of the nanoparticles, exemplified by the linear scaling of the MSD with delay time and by the q^{-2} dependence of the relaxation time obtained from the image structure function. Moreover, the averaged relative decay length $\langle \gamma(\Delta t)/\gamma_0(\Delta t) \rangle$, where $\gamma_0(\Delta t)$ corresponds to the decay length for the free diffusion case and the averaging is over the delay times studied here, scaled nearly linearly with void fraction and confinement parameter (Figure 9), as also found for the relative diffusivity in Figure 5. Finally, we observe that the magnitude of the decrease in the averaged relative decay length is *quantitatively* similar to that in the relative diffusivity.

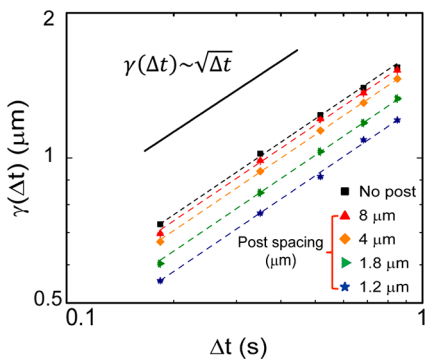


Figure 8. Decay length $\gamma(\Delta t)$ as a function of the delay time for 400 nm nanoparticles diffusing freely (black square) and in post arrays with $S = 8 \mu\text{m}$, $\zeta = 0.051$ (red up triangle), $S = 4 \mu\text{m}$, $\zeta = 0.105$ (orange diamond), $S = 1.8 \mu\text{m}$, $\zeta = 0.237$ (olive right triangle) and $S = 1.2 \mu\text{m}$, $\zeta = 0.354$ (navy star). $\gamma(\Delta t)$ scales as $\Delta t^{0.5}$. The error bars are smaller than the symbols.

The slowed dynamics of the nanoparticles, the stretched exponential behavior of the relaxation process, the linear decrease of the stretching exponent, and the linear decrease of the averaged relative decay length with increased confinement are manifestations of the impact of the cylindrical post arrays on the dynamics of the nanoparticles. The decrease in diffusivity follows linearly with the increase in confinement, and thus, confinement effects alone are sufficient to explain the slowing of dynamics. For even the smallest post spacing ($\sim 1.2 \mu\text{m}$) and the largest particles (400 nm diameter) studied, however, the dynamics remained Fickian in nature. The observation of Fickian yet anomalous diffusion is similar to that of Granick and co-workers for two classes of systems: colloidal particles diffusing along linear phospholipid bilayer tubes with radii similar to that of the colloidal particles, and colloidal beads diffusing in entangled fiber networks.³⁸ Granick and co-workers attributed non-Gaussian yet Fickian dynamics in these two systems to slowly varying fluctuations in a heterogeneous environment.³⁹ In the systems described in this paper, however, we cannot categorically determine the origins of the anomalously stretched dynamics. We expect that both heterogeneous environments (*i.e.*, varying proximity of the nanoparticles to the nanoposts arranged on a square lattice), on the scale of a few particle diameters, and caging-induced confinement and approach to vitrification, on the scale of the particle size, give rise to these dynamics. While the current work provides a systematic study of the changes in the relaxation spectra induced by confinement heterogeneity and by the approach to a confinement-induced vitrification, it does not allow us to distinguish between these two phenomena.

CONCLUSIONS

Our measurements, summarized in Figures 5–8, revealed two characteristic features of nanoparticle diffusion in post arrays: slowing of dynamics, shown by the decrease in the average diffusion coefficient, and the emergence of multiple relaxation processes

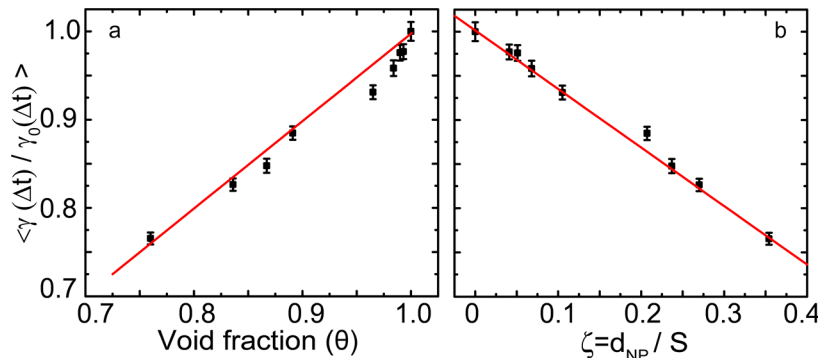


Figure 9. Averaged relative decay length $\langle \gamma(\Delta t)/\gamma_0(\Delta t) \rangle$ as a function of (a) void fraction θ and (b) confinement parameter $\zeta (=d_{NP}/S)$, measured by single particle tracking for aqueous dispersions of nanoparticles of diameter of 400 nm. The relative decay length scales linearly with θ and ζ .

TABLE 1. Post Spacing, Height, and Void Fraction for Nanoparticles Diffusing in Different Post Arrays Described in This Paper

designed spacing (μm)	measured spacing (μm)	height (μm)	void fraction θ			confinement $\zeta = d_{\text{NP}}/S$		
			200 nm	300 nm	400 nm	200 nm	300 nm	400 nm
10	9.79 ± 0.05	10.0 ± 0.1	0.99 ₆	0.99 ₅	0.99 ₃	0.02 ₁	0.03 ₁	0.04 ₁
8	7.79 ± 0.06	10.3 ± 0.1	0.99 ₄	0.99 ₃	0.99 ₀	0.02 ₆	0.03 ₉	0.05 ₁
6	5.86 ± 0.03	10.0 ± 0.1	0.99 ₀	0.98 ₈	0.98 ₄	0.03 ₄	0.05 ₁	0.06 ₈
4	3.82 ± 0.04	10.2 ± 0.1	0.97 ₉	0.97 ₃	0.96 ₅	0.05 ₂	0.07 ₉	0.10 ₅
2	1.93 ± 0.06	11.6 ± 0.1	0.93 ₅	0.91 ₅	0.89 ₁	0.10 ₄	0.15 ₅	0.20 ₇
1.8	1.69 ± 0.07	11.8 ± 0.1	0.92 ₀	0.89 ₅	0.86 ₇	0.11 ₈	0.17 ₈	0.23 ₇
1.6	1.48 ± 0.15	11.9 ± 0.1	0.90 ₁	0.87 ₁	0.83 ₆	0.13 ₅	0.20 ₃	0.27 ₀
1.2	1.13 ± 0.10	12.1 ± 0.1	0.85 ₅	0.81 ₁	0.76 ₀	0.17 ₇	0.26 ₅	0.35 ₄

with a spectrum of relaxation times, shown by the decrease in the stretching exponent. These features suggest an intriguing connection between confined dynamics of nanoparticles and their relationship to the systematic variation in confinement heterogeneity and to confinement-induced vitrification.²⁹ In ref 29, the anomalous and non-Gaussian dynamics of dense liquids confined in porous media could be described by mode-coupling theory, which is commonly used to describe the slowing of dynamics near the glass transition. In this interpretation, the porous medium acts as a frozen host structure, and the anomalous slowed and

stretched dynamics reflect the interplay between this underlying spatial structure and an approach to vitrification.²⁹ In our experiments, in which the confinement was relatively modest, the diffusive dynamics became slower (by ~25%) and the stretching exponent decreased (to 0.7). We expect that similar measurements in more extreme confinements, as well as those in which particle–surface interactions or pore connectivity are varied, will distinguish between heterogeneity and vitrification and thereby provide unique insight into the changing nature of the dynamics of nanoparticles in complex media.

METHODS

Nanoparticle Dispersions. Fluo-max dyed red aqueous fluorescent polystyrene particles with diameter (d_{NP}) of 200, 300, and 400 nm were purchased from Thermo Fisher Scientific CDD. The as-received dispersions (with 1 wt % of nanoparticles) were diluted with deuterium oxide (Sigma-Aldrich) to a volume fraction of $\varphi = 1 \times 10^{-4}$, corresponding to number densities of $2.2 \times 10^{10} \text{ mL}^{-1}$, $6.7 \times 10^9 \text{ mL}^{-1}$, and $2.8 \times 10^9 \text{ mL}^{-1}$ for 200, 300, and 400 nm nanoparticles, respectively. A detailed description of these materials and the sample preparation protocol can be found in ref 30.

Fabrication and Characterization of Cylindrical Nanopost Arrays. To systematically explore the effect of confinement by nanoposts, we fabricated individual arrays of posts of area of $250 \times 250 \mu\text{m}^2$ in which the post spacing was held constant. Rectangular cylindrical post arrays of constant diameter (d_p) 500 nm separated by spacing (S) of 1.2 to 10 μm , as shown in Figure 1, were prepared on silicon wafers using methods developed previously.²⁸ Briefly, ZEP520A photoresist was coated on a 4 in. *p*-type silicon wafer (100) at 6000 rpm for 45 s and baked at 180 °C for 2 min. Square arrays with post patterns were produced by electron beam lithography (JBX-9300 FS). The post patterns were then developed in xylene for 30 s, rinsed with isopropyl alcohol (IPA), and dried with N₂. A 15 nm layer of Cr was deposited using a dual gun electron beam evaporation vacuum chamber (Thermionics, Port Townsend, WA) at the metal evaporation rate of 1 Å/s. Photoresist lift off (by sonication of the wafer in acetone for 2 min) was performed to ensure the removal of the resist and the majority of the Cr film. Cylindrical posts of 10 μm height were produced using cryogenic silicon etching by an Oxford Plasmalab system 100 (etched by SF₆ and O₂, plasma at –110 °C, with an optimized flow rate of 18 sccm of O₂) for 4 min. Finally, a uniform 10 nm thick SiO₂ layer was deposited by atomic layer deposition. This fabrication process resulted in a hydroxyl coated silica posts arranged in a regular array that did not offer strong specific interactions with the

polystyrene nanoparticles that had a small extent of carboxylate functionality to help disperse in water.

The geometrical characteristics of the post array (i.e., the post spacing and height) were measured by scanning electron microscopy and are summarized in Table 1. We additionally report two metrics that parametrize the confinement experienced by the nanoparticles. First, we calculated the area-based void fraction θ for each of the dilute nanoparticle dispersions as

$$\theta = \frac{(S+d_p)^2 - \frac{\pi}{4}(d_p+d_{\text{NP}})^2}{(S+d_p)^2} \quad (5)$$

where d_p is the diameter of the post, d_{NP} is the diameter of the nanoparticles, and S is the spacing between posts. The second term in eq 5 accounted for the area within half a particle diameter of each post that was inaccessible to the centers of the nanoparticles. Second, we calculated a confinement parameter $\zeta = d_{\text{NP}}/S$, the ratio of the nanoparticle diameter to the spacing between posts, to capture the topological confinement of the particles in the array. A value of 0 for ζ corresponds to the unconfined case, while a value of 1 corresponds to complete confinement.

Experimental Procedure for Study of Nanoparticle Diffusion in Post Arrays. Dispersions of nanoparticles were introduced into silicon-based microchannel arrays using a pipet. A rectangular cover glass with dimensions of $48 \times 65 \text{ mm}^2$ (thickness 0.13–0.17 mm, Gold Seal) and an epoxy-based adhesive (Devcon) was used to seal the microchannel and thereby form a hermetic system. Nanoparticles diffusing in the sealed systems were imaged on a Leica DM4000 inverted microscope with a 100× oil immersion objective (HCX PL APO, numerical aperture of 1.40) and a pixel size of $0.195 \pm 0.002 \mu\text{m}/\text{pixel}$ using a high speed AOS Camera (AOS Technologies AG). We used reflected light to precisely locate each rectangular post array that was patterned on the microchannel, as the opacity of the silicon wafer precluded the use of transmitted light. We then switched

to fluorescence mode to image the nanoparticle dispersions. In the microscopy experiments, we collected 4200 images over an area of $124.8 \times 93.6 \mu\text{m}^2$ (corresponding to 640 pixels \times 480 pixels) at a frame rate of 63 (for 200 nm diameter nanoparticles) or 120 (300 and 400 diameter nanoparticles) frames per second (fps). This imaging protocol allowed us to access delay-time scales ranging from 0.0083 to 35 s (at 120 fps) for the 200 diameter NPs and 0.0158 to 67 s (at 63 fps) for the larger NPs. Because the field of view was smaller than the post array and care was taken to center the field of view with that of the array, edge effects were precluded from our data collection and analysis.

Image Analysis. To measure the diffusive dynamics of the nanoparticles in cylindrical post arrays with varied post spacing, we implemented a differential dynamic microscopy (DDM) algorithm to analyze the fluctuations in light intensity in a time series of fluorescence micrographs.^{40,41} We previously showed³⁰ that fluorescence- and brightfield-based DDM provided equivalent data to those obtained from dynamic light scattering and enabled measurements over a broader concentration range of scatterers and over a broader range of the magnitude of the scattering vector (q). Briefly, we calculated the azimuthally averaged image structure function (ISF) $D(q, \Delta t)$ from the Fourier analysis of a delay-time series of difference images. The Fourier transforms of the difference images were nearly isotropic for all delay times studied in this work, thereby validating the use of an azimuthally averaged $D(q, \Delta t)$ and a single particle diffusion coefficient (Supporting Information, Figure S1). We fitted the structure factor to a generalized model, $D(q, \Delta t) = A(q)[1 - f(q, \Delta t)] + B(q)$, and extracted a q -dependent relaxation time $\tau(q)$ from the intermediate scattering function $f(q, \Delta t)$. Nonlinear least-squares fitting was performed using the Levenberg–Marquardt algorithm, as implemented in Origin (OriginLab, Northampton, MA). We calculated the particle diffusivity as $D_m = 1/\tau(q)q^2$ from the slope of $\tau(q)$ versus q^2 .

To verify our DDM measurements, we used a single particle-tracking (SPT) algorithm to track the 400 nm diameter nanoparticles as they diffused in the post arrays.⁴² Briefly, we located the particle centroids to within 40 nm and linked the particle positions into trajectories. From the trajectories, we calculated the one-dimensional ensemble-averaged mean squared displacement ($\text{MSD}(\Delta x^2, \Delta t) = \langle (x(t+\Delta t) - x(t))^2 \rangle$) of the particles over time, where the brackets indicate an average over all particles in the system, and the probability distribution of particle displacements $G_s(\Delta x, \Delta t)$.

Conflict of Interest: The authors declare no competing financial interest.

Acknowledgment. This publication is based on work supported in part by Award No. KUS-C1-018-02, made by King Abdullah University of Science and Technology (KAUST). R.K. and K.H. acknowledge the partial support of the Gulf of Mexico Research Initiative (Consortium for Ocean Leadership Grant SA 12-05/GoMRI-002). J.C.C. is supported by the American Chemical Society Petroleum Research Fund (52537-DNI7) and the National Science Foundation (DMR-1151133). A portion of this research was conducted at the Center for Nanophase Materials Sciences, which is sponsored at Oak Ridge National Laboratory by the Scientific User Facilities Division, Office of Basic Energy Sciences, U.S. Department of Energy.

Supporting Information Available: Diffusion data for 200 and 300 nm particles in the post arrays and a mathematical description of the consequences of the stretched exponential model are presented. This material is available free of charge via the Internet at <http://pubs.acs.org>.

REFERENCES AND NOTES

- Grattoni, A.; Gill, J.; Zabre, E.; Fine, D.; Hussain, F.; Ferrari, M. Device for Rapid and Agile Measurement of Diffusivity in Micro-and Nanochannels. *Anal. Chem.* **2011**, *83*, 3096–3103.
- Stylianopoulos, T.; Poh, M.-Z.; Insin, N.; Bawendi, M. G.; Fukumura, D.; Munn, Lance L.; Jain, R. K. Diffusion of Particles in the Extracellular Matrix: The Effect of Repulsive Electrostatic Interactions. *Biophys. J.* **2010**, *99*, 1342–1349.
- Gulyaev, A. E.; Gelperina, S. E.; Skidan, I. N.; Antropov, A. S.; Kivman, G. Y.; Kreuter, J. Significant Transport of Doxorubicin into the Brain with Polysorbate 80-Coated Nanoparticles. *Pharm. Res.* **1999**, *16*, 1564–1569.
- Koziara, J. M.; Lockman, P. R.; Allen, D. D.; Mumper, R. J. Paclitaxel Nanoparticles for the Potential Treatment of Brain Tumors. *J. Controlled Release* **2004**, *99*, 259–269.
- Bradford, S. A.; Yates, S. R.; Bettahar, M.; Simunek, J. Physical Factors Affecting the Transport and Fate of Colloids in Saturated Porous Media. *Water Resour. Res.* **2002**, *38*, 1327–1339.
- Davit, Y.; Byrne, H.; Osborne, J.; Pitt-Francis, J.; Gavaghan, D.; Quintard, M. Hydrodynamic Dispersion within Porous Biofilms. *Phys. Rev. E* **2013**, *87*, 012718.
- Peulen, T. O.; Wilkinson, K. J. Diffusion of Nanoparticles in a Biofilm. *Environ. Sci. Technol.* **2011**, *45*, 3367–3373.
- Ponnappati, R.; Karazincir, O.; Dao, E.; Ng, R.; Mohanty, K. K.; Krishnamoorti, R. Polymer Functionalized Nanoparticles for Improving Waterflood Sweep Efficiency – Characterization and Transport Properties. *Ind. Eng. Chem. Res.* **2011**, *50*, 13030–13036.
- Wu, M. J.; Xiao, F.; Johnson-Paben, R. M.; Retterer, S. T.; Yin, X. L.; Neeves, K. B. Single-and Two-Phase Flow in Microfluidic Porous Media Analogs based on Voronoi Tessellation. *Lab Chip* **2012**, *12*, 253–261.
- Goldman, A.; Cox, R. G.; Brenner, H. Slow Viscous Motion of a Sphere Parallel to a Plane Wall—I Motion Through a Quiescent Fluid. *Chem. Eng. Sci.* **1967**, *22*, 637–651.
- Eral, H. B.; Oh, J. M.; van den Ende, D.; Mugele, F.; Duits, M. H. G. Anisotropic and Hindered Diffusion of Colloidal Particles in a Closed Cylinder. *Langmuir* **2010**, *1*–8.
- Eichmann, S. L.; Anekal, S. G.; Bevan, M. A. Electrostatically Confined Nanoparticle Interactions and Dynamics. *Langmuir* **2008**, *24*, 714–721.
- Choi, C. K.; Margraves, C. H.; Kihm, K. D. Examination of Near-Wall Hindered Brownian Diffusion of Nanoparticles: Experimental Comparison to Theories by Brenner (1961) and Goldman *et al.* (1967). *Phys. Fluids* **2007**, *19*, 103305.
- Diamant, H. Hydrodynamic Interaction in Confined Geometries. *J. Phys. Soc. Jpn.* **2009**, *78*, 041002.
- Fakhri, N.; Mackintosh, F. C.; Lounis, B.; Cognet, L.; Pasquali, M. Brownian Motion of Stiff Filaments in a Crowded Environment. *Science* **2010**, *330*, 1804–1807.
- Carmen, J.; Goel, G.; Pond, M. J.; Errington, J. R.; Truskett, T. M. Enhancing Tracer Diffusivity by Tuning Intercapillary Interactions and Coordination Shell Structure. *Soft Matter* **2012**, *8*, 4083–4090.
- Beschieru, V.; Rathke, B.; Will, S. Particle Diffusion in Porous Media Investigated by Dynamic Light Scattering. *Micro-porous Mesoporous Mater.* **2009**, *125*, 63–69.
- Amblard, F.; Maggs, A. C.; Yurke, B.; Pargellis, A.; Leibler, S. Subdiffusion and Anomalous Local Viscoelasticity in Actin Networks. *Phys. Rev. Lett.* **1996**, *77*, 4470–4473.
- Babu, S.; Gimel, J. C.; Nicolai, T. Tracer Diffusion in Colloidal Gels. *J. Phys. Chem. B* **2008**, *112*, 743–748.
- Egorov, S. A. Anomalous Nanoparticle Diffusion in Polymer Solutions and Melts: A Mode-Coupling Theory Study. *J. Chem. Phys.* **2011**, *134*, 084903.
- Omari, R. A.; Aneese, A. M.; Grabowski, C. A.; Mukhopadhyay, A. Diffusion of Nanoparticles in Semidilute and Entangled Polymer Solutions. *J. Phys. Chem. B* **2009**, *113*, 8449–8452.
- Pryamitsyn, V.; Ganesan, V. Dynamics of Probe Diffusion in Rod Solutions. *Phys. Rev. Lett.* **2008**, *100*, 128302.
- Wong, I. Y.; Gardel, M. L.; Reichman, D. R.; Weeks, E. R.; Valentine, M. T.; Bausch, A. R.; Weitz, D. A. Anomalous Diffusion Probes Microstructure Dynamics of Entangled F-actin Networks. *Phys. Rev. Lett.* **2004**, *92*, 178101.
- Ghosh, P. K.; Hänggi, P.; Marchesoni, F.; Martens, S.; Nori, F.; Schimansky-Geier, L.; Schmid, G. Driven Brownian Transport Through Arrays of Symmetric Obstacles. *Phys. Rev. E* **2012**, *85*, 011101.

25. Cherdhirankorn, T.; Retsch, M.; Jonas, U.; Butt, H. J.; Koynov, K. Tracer Diffusion in Silica Inverse Opals. *Langmuir* **2010**, *26*, 10141–10146.
26. Raccis, R.; Nikoubashman, A.; Retsch, M.; Jonas, U.; Koynov, K.; Butt, H.-J.; Likos, C. N.; Fytas, G. Confined Diffusion in Periodic Porous Nanostructures. *ACS Nano* **2011**, *5*, 4607–4616.
27. Baumann, T.; Werth, C. J. Visualization and Modeling of Polystyrol Colloid Transport in a Silicon Micromodel. *Vadose Zone J.* **2004**, *3*, 434–443.
28. Choi, C. K.; Fowlkes, J. D.; Retterer, S. T.; Siuti, P.; Iyer, S.; Doktycz, M. J. Surface Charge- and Space-Dependent Transport of Proteins in Crowded Environments of Nano-tailored Posts. *ACS Nano* **2010**, *4*, 3345–3355.
29. Spanner, M.; Schnyder, S.; Höfling, F.; Voigtmann, T.; Franosch, T. Dynamic Arrest in Model Porous Media—Intermediate Scattering Functions. *Soft Matter* **2013**, *9*, 1604–1611.
30. He, K.; Spannuth, M.; Conrad, J. C.; Krishnamoorti, R. Diffusive Dynamics of Nanoparticles in Aqueous Dispersions. *Soft Matter* **2012**, *8*, 11933–11938.
31. Ediger, M. Spatially Heterogeneous Dynamics in Super-cooled Liquids. *Annu. Rev. Phys. Chem.* **2000**, *51*, 99–128.
32. Williams, G.; Watts, D. C. Non-Symmetrical Dielectric Relaxation Behaviour Arising from a Simple Empirical Decay Function. *Trans. Faraday Soc.* **1970**, *66*, 80–94.
33. Dix, J. A.; Verkman, A. S. Crowding Effects on Diffusion in Solutions and Cells. *Annu. Rev. Biophys.* **2008**, *37*, 247–263.
34. Roosen-Runge, F.; Hennig, M.; Zhang, F. J.; Jacobs, R. M. J.; Sztucki, M.; Schober, H.; Seydel, T.; Schreiber, F. Protein Self-Diffusion in Crowded Solutions. *Proc. Natl. Acad. Sci. U.S.A.* **2011**, *108*, 11815–11820.
35. Johnston, D. Stretched Exponential Relaxation Arising from a Continuous Sum of Exponential Decays. *Phys. Rev. B* **2006**, *74*, 184430.
36. Kubo, R. The Fluctuation-Dissipation Theorem. *Rep. Prog. Phys.* **1966**, *29*, 255–284.
37. Lindsey, C. P.; Patterson, G. D. Detailed Comparison of the Williams-Watts and Cole-Davidson Functions. *J. Chem. Phys.* **1980**, *73*, 3348–3357.
38. Wang, B.; Anthony, S. M.; Bae, S. C.; Granick, S. Anomalous yet Brownian. *Proc. Natl. Acad. Sci. U.S.A.* **2009**, *106*, 15160–15164.
39. Wang, B.; Kuo, J.; Bae, S. C.; Granick, S. When Brownian Diffusion is not Gaussian. *Nat. Mater.* **2012**, *11*, 481–485.
40. Cerbino, R.; Trappe, V. Differential Dynamic Microscopy: Probing Wave Vector Dependent Dynamics with a Microscope. *Phys. Rev. Lett.* **2008**, *100*, 188102.
41. Cerbino, R.; Vailati, A. Near-Field Scattering Techniques: Novel Instrumentation and Results from Time and Spatially Resolved Investigations of Soft Matter Systems. *Curr. Opin. Colloid Interface Sci.* **2009**, *14*, 416–425.
42. Crocker, J. C.; Grier, D. G. Methods of Digital Video Microscopy for Colloidal Studies. *J. Colloid Interface Sci.* **1996**, *179*, 298–310.